

Automatic segmentation of agricultural objects in dynamic outdoor environments

Amy Tabb^{1,*}

USDA-ARS-AFRS, West Virginia, USA

Henry Medeiros

Marquette University, Wisconsin, USA

Abstract

Segmentation in dynamic outdoor environments can be difficult when the illumination levels and other aspects of the scene cannot be controlled. Specifically in agricultural contexts, a background material is often used to shield a camera's field of view from other rows of crops. In this paper, we describe a method that uses superpixels to determine low texture regions of the image that correspond to the background material, and then show how this information can be integrated with the color distribution of the image to compute optimal segmentation parameters to segment objects of interest. Quantitative and qualitative experiments demonstrate the suitability of this approach for dynamic outdoor environments, specifically for tree reconstruction and apple flower detection applications.

Keywords: segmentation; agricultural automation; tree recognition; outdoor vision

1. Introduction

Segmentation is a key step in many automation contexts, and when the result is accurate, can reduce the amount of information presented to subsequent steps of an autonomous computer vision system. This paper describes a method for segmentation of a mobile background unit from tree regions in an orchard setting as part of an automated pipeline to reconstruct the shape of leafless trees for robotic pruning and phenotyping [1, 2, 3]. Since the images are acquired outdoors, illumination conditions are not stable and may change rapidly and widely. Furthermore, the entire process is automated, and hundreds of images must be acquired per tree. Hence, the segmentation method must be robust and not require parameter tuning either over the course of acquiring images for one tree or over an entire day of data acquisition. Since our goal is to use the segmentation step as part of an automation application, the method must also be fast.

The ability to robustly extract the silhouettes of objects of interest is generally an important step in the generation of three-dimensional models of complex objects such as trees ([1]) and may form a preprocessing step for other tasks, such as flower detection. Existing silhouette extraction techniques based solely on thresholding and morphological characteristics of the object of interest, however, tend to generate unsatisfactory results, particularly with respect to segmentation. This

problem, as with most computer vision tasks, is further aggravated in dynamic environments, which include situations such as drastically varying illumination conditions. Hence, we propose a novel method to segment an object (in this case a tree) from a low-texture background, which is robust to significant illumination changes.

The segmentation method proposed in this paper assumes an item of interest in a image is positioned in front of a background material of homogeneous color. It locates the low texture regions of the image using superpixels and models them using a Gaussian Mixture Model (GMM). Pixels in the image are classified according to the GMM and a mask of the background material region is created. The method is fully autonomous and does not require user input or training, other than initial setting of thresholds. The main contribution of this work is an unsupervised method to segment foreground objects in images that is sufficiently robust to operate with various models of cameras under natural outdoor illumination conditions and is fast enough to be used in automation contexts. The method is verified through quantitative and qualitative experiments as well as comparisons to alternative approaches based on Otsu's method and adaptive thresholding mechanisms.

The remainder of this paper is organized as follows. Section 2 presents a brief overview of methods for the segmentation of foreground objects with a particular focus on agricultural applications. Section 3 describes our proposed approach. A comprehensive evaluation comparing the performance of our methods to alternative approaches to foreground object segmentation is given in Section 4. Finally, Section 5 concludes the paper and discusses possible future research directions.

*Corresponding author

Email address: amy.tabb@ars.usda.gov (Amy Tabb)

¹Mention of trade names or commercial products in this publication is solely for the purpose of providing specific information and does not imply recommendation or endorsement by the U.S. Department of Agriculture. USDA is an equal opportunity provider and employer. A. Tabb acknowledges the support of US National Science Foundation grant number IOS-1339211.

2. Related work

There is a significant amount of related work on segmentation in dynamic environments for the purposes of foreground detection as recently reviewed by Bouwmans [4]. Traditionally, in foreground detection, the assumption is that the background can be modeled because the cameras observing a scene are not moving. The background image hence remains relatively static and objects that move with respect to the camera are considered part of the foreground. A popular approach for foreground, or motion, detection is that of Stauffer and Grimson [5], in which each image pixel is modeled as a mixture of Gaussians. Various extensions of [5], from a hierarchical approach for real-time execution [6] to models that consider non-Gaussian distributions [7], have been explored as well for the context of relatively static backgrounds. In the scenarios under consideration in this work, however, the background may change drastically, so motion detection approaches are not applicable.

In the agricultural context, many applications require the segmentation of plants from soil with a moving camera; this problem has been recently surveyed by Hamuda *et al.* [8]. Concerning applications of tree segmentation, Byrne and Singh [9] use co-occurrence statistics to oversegment images into tree versus non-target tree regions for use in autonomous diameter measurement for a automated forestry application. In a similar application, Ali [10] uses a combination of color and texture features fed into an artificial neural network and k-nearest neighbor classifiers to perform classification of pixels into tree and non-tree classes. Like our work, Botterill *et al.* in [11] also use a blue background for their design of a robotic grapevine pruner. However, their unit is an over-the-row unit and does not have to navigate the illumination challenges we do. In [11], training data is hand-labelled into three classes: background, wire, foreground, and color features and used to train a support vector machine (SVM), which is later used for classification. Zheng *et al.* [12] address segmenting root material from gels by using a harmonic background subtraction method with hysteresis thresholding.

Mobile background units, such as the ones used in our work, have been used for various purposes, from apple harvest [13, 14, 15], to grape pruning [11], and tree shape estimation [1, 2, 3]. The advantage of using such a background, especially with trees planted in rows, is that the influence of neighboring rows of trees is eliminated. Some units, such as those shown in [11, 13, 14, 15], are over-the-row units to shield the imaging area from variations in illumination from the environment. Another option has been to acquire images at night with artificial illumination to create a static background and mitigate illumination variation, such as [16] to detect cherry, [17] to detect tree branches using RGB-D cameras, and [18, 19] to detect apple fruit. Nighttime-only operation, however, significantly restricts the practical applicability of any agricultural robotic system.

3. Method description

We assume a low-texture background object is present in each image, and we model the hue component of this back-

ground object according to a Gaussian mixture model with k components: $p(h) = \sum_{j=1}^k w_j \mathcal{N}(\mu_j, \sigma_j^2)$, where μ_j and σ_j are the mean and variance of the j -th mixture component and w_j is its corresponding weight. In the following steps, we show how we estimate this distribution and then use it to assign probabilities for each pixel in the image. We also assume that the object of interest is positioned between the background object and the camera (see Figure 1a). Regions that extend beyond the background object are truncated. Algorithm 1 shows an overview of the proposed approach. Each step of the algorithm is explained in detail in the following subsections. While the first two steps of the algorithm are independent and can be performed in parallel, the remaining steps depend upon one another and hence need to be performed in order. The sequence of steps is illustrated in Figure 1.

Algorithm 1 Proposed segmentation approach

Input: Image in hue-saturation-value (HSV) color space

Output: Segmented image

- 1: Compute the set of superpixels \mathbb{S} using the SEEDS method [20] and find the subset $\mathbb{R} \subset \mathbb{S}$ of low-texture superpixels.
 - 2: Generate a binary image T , by thresholding the hue channel using Otsu’s algorithm.
 - 3: Determine GMM $p(h) = \sum_{j=1}^k w_j \mathcal{N}(\mu_j, \sigma_j^2)$, which represents the background, based on \mathbb{R} and T .
 - 4: Generate label image L by assigning labels to individual output pixels according to the GMM.
 - 5: Create a mask to eliminate regions outside of the background object.
-

3.1. Step 1: Computation of low-texture superpixels

The first step of our approach consists of converting the image to the HSV color space and partitioning it into superpixels. We have chosen to compute the superpixels using the superpixels extracted via energy-driven sampling (SEEDS) method proposed in [20] and implemented in OpenCV [21]. In this superpixel approach, the image is divided into a grid pattern, which serves as initial superpixel assignment. The superpixel assignments are refined by iteratively modifying their boundaries.

Starting from an initial superpixel division of a grid, in SEEDS, pixels change label as a result of a maximizing a cost function based on a color likelihood term and optional shape prior. We set the parameters of the SEEDS algorithm such that low texture regions have superpixels whose shape is unchanged from the initial grid assignment. That is, let \mathbb{S} be the set of superpixels generated by SEEDS. Then there is a set of superpixels $\mathbb{R} \subset \mathbb{S}$, which are rectangular in shape. These are the superpixels which are unchanged from the initial assignment and correspond to low-texture regions. Figures 1a and 1b show the original RGB image and the hue channel of its corresponding HSV representation. Figure 1c then shows the superpixels generated according to our proposed procedure. As the image shows, most superpixels on the background object are rectangular in shape.

3.2. Step 2: Generation of thresholded hue image using Otsu's algorithm

We then generate the binary image T by thresholding the hue channel of the HSV image using Otsu's algorithm [22]. In the binary image, pixels with value below the threshold value are black and the remaining pixels are white. As explained in the next section, the image T is used to generate hypotheses of low-texture regions in the image, since the color of the low-texture background object is relatively constant. In our application, the blue background object has a higher hue value than other common colors in the images such as brown, gray, or green, which facilitates the application of the proposed approach. We are not limited to a single background color though. As long as the hue value of the majority of the pixels in the background differ from those of the foreground object, T can be generated using multi-level thresholding algorithms [23].

3.3. Step 3: Estimation of the distribution of the background

The first two steps consisted of coarse detectors for the blue background. The superpixel approach in step one finds low texture regions, while T found in step two indicates regions likely to be the background judging by relative hue as compared to the rest of the image. We now combine the information from these two steps to generate a more robust background detector.

We determine regions where T overlaps superpixels in \mathbb{R} using the procedure summarized in Algorithm 2. Briefly, the algorithm iterates through the superpixels in \mathbb{R} . If the percentage of white pixels in the corresponding area of the thresholded image T exceeds a value $\zeta \in [0, 1]$, then the superpixel is added to a set \mathbb{B} . The set \mathbb{B} hence consists of all the superpixels which belong to a low-texture region as determined by the SEEDS algorithm *and* by its constant color.

All of the pixel locations in the set of superpixels \mathbb{B} are then used to estimate the probability distribution of the background pixels. Let h_i be the value of the i th pixel in the hue image. We assume the pixel intensities of the background material regions over the whole image can be represented by a mixture of k normal distributions. That is, the probability density is

$$p(h_i) = \sum_{j=1}^k w_j * \mathcal{N}(h_i, \mu_j, \sigma_j^2) \quad (1)$$

where \mathcal{N} is the Gaussian probability density function

$$\mathcal{N}(h_i, \mu_j, \sigma_j^2) = \frac{1}{\sigma_j \sqrt{2\pi}} e^{-\frac{(h_i - \mu_j)^2}{2\sigma_j^2}} \quad (2)$$

The parameters of the distribution, k , w_j , μ_j and σ_j , may be obtained using the expectation-maximization (E-M) algorithm from the pixels in \mathbb{B} . Initial values of the distribution are estimated using k-means clustering. However, E-M can take a long time to converge with a large number of samples, as is the case when the number of pixels in \mathbb{B} is large. We used a faster approach than E-M to create a GMM with satisfactory results as follows. Essentially, the information from superpixels are grouped into clusters, and then the components of the GMM

are computed from the clusters using all of the pixels in the superpixels that compose those clusters. First, the sample means of the individual superpixels in \mathbb{B} were clustered into k groups using the kmeans++ algorithm [24]. Then, from these clusters, the means and variances of the k clusters were determined from all of the pixels contained in all superpixels contained by that cluster. Finally, the weights were computed, where if the number of superpixels in cluster j is s_j , then $w_j = s_j/|\mathbb{B}|$.

Algorithm 2 Determination of background pixels

Input: Set \mathbb{R} of low-texture superpixels and thresholded hue image T

Output: Set \mathbb{B} of background superpixels

- 1: $\mathbb{B} = \{\}$
 - 2: **for** each superpixel $r_i \in \mathbb{R}$ **do**
 - 3: $t_i =$ number of white pixels in T for the region of r_i .
 - 4: **if** $t_i/\text{area}(r_i) > \zeta$ **then**
 - 5: $\mathbb{B} = \mathbb{B} \cup r_i$
-

3.4. Step 4: Pixel label assignment based on the background distribution

The hue image is compared to the GMM to generate an image of pixel labels L as follows. Let $p(h_i)$ be the likelihood of h_i as predicted by the Gaussian Mixture Model, and let p_t be a corresponding threshold value. Then, the pixel labels L_i are created according to

$$L_i = \begin{cases} 1, & p(h_i) \leq p_t \\ 0 & p(h_i) > p_t \end{cases} \quad (3)$$

Since the pixels in the set \mathbb{B} were used to generate the background model, their labels can be automatically assigned to $L_i = 0$ during model computation (Step 3) and do not need to be revisited in this step. This has the dual benefit of reducing computation time as well as avoiding spurious noisy pixels in \mathbb{B} that would make the overall method more sensitive to the value of the threshold p_t .

3.5. Step 5: Create mask to eliminate regions outside the background object

The final step creates a mask image M , in which regions including the object of interest, in this case the tree, and the background object, are labeled white and all other regions are labeled black. This mask is generated over the course of three steps. First, M is set to the inverse of L and small connected components with area smaller than a threshold of ϵ_a are removed from M . These components typically represent false background detections in the sky or surrounding natural environment. It remains to connect the white sections of M . The contours for each connected component are found, and then for each point on the contour, the closest point on a different contour is found and a line drawn between the contours. To conclude, all of the holes are filled in M .

The mask is applied to the pixel label image L so that if the i th pixel of M is 0, then this pixel is outside the region of interest and the corresponding pixel in L is labeled accordingly.

In this application, we label those pixels 0 and the pixels inside the region of interest are labeled 1. Alternatively, our method allows pixels that do not belong to the region of interest to be labeled using a special marker value so that downstream processing steps could recognize them and treat them accordingly.

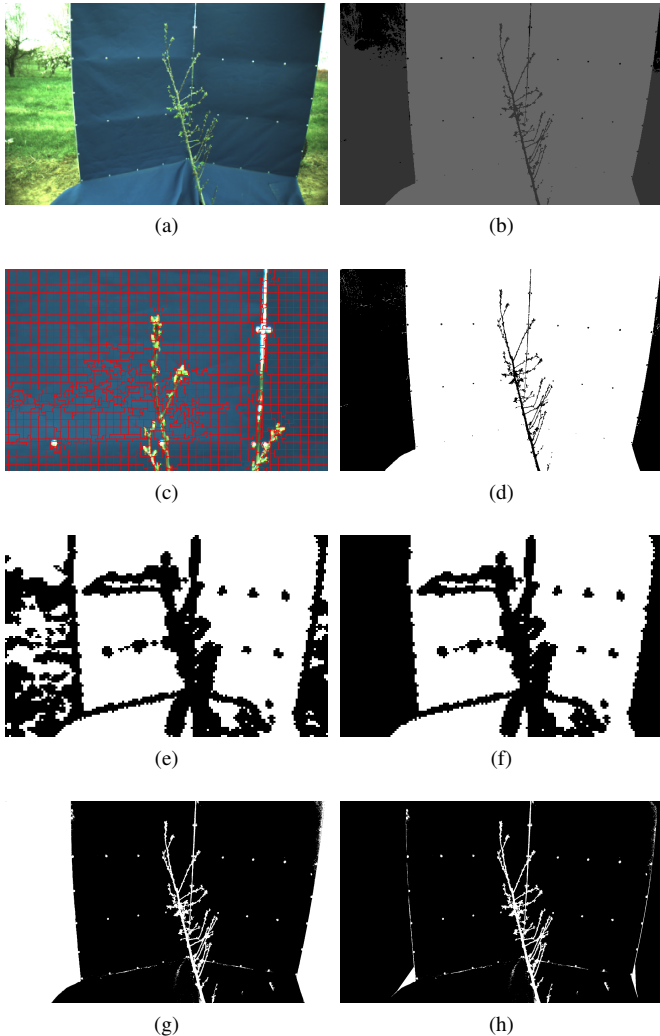


Figure 1: **[Best viewed in color]** (a) Original RGB image showing the object of interest (tree) in front of the background object. (b) Hue channel. (c) Close-up of portion of the original image (top portion of branch) with superpixels overlaid in red. (d) Threshold result from step 2 (T). (e) The set of superpixels \mathbb{R} is shown in white, indicating low texture regions. (f) Set of superpixels \mathbb{B} , where white pixels indicate locations where the GMM is estimated in the hue image. (g) Label image L after label assignment step. (h) L after application of the mask in step 5.

4. Experiments

We evaluated our proposed approach on six datasets containing a total of 1001 images. As shown in Table 2, five of these datasets were acquired outdoors with different camera models and resolutions, and one of them was acquired indoors. Most datasets consisted of images collected by multiple cameras. These datasets reflect a range of illumination conditions. Although no extensive parameter optimization was carried out, we

found that the following parameters showed satisfactory performance for all of the datasets: threshold parameter $\zeta = 0.8$, mask generation parameter $\epsilon_a = 2000$ and threshold $p_t = 0.003$. The number of distributions in the GMM was set to $k = 10$. The SEEDS superpixel was configured for number iterations = 10, number histogram bins = 2, number of superpixels = 16,000, number of levels = 1, prior = 0, and double step = false. Also, basic morphological operations could have been applied to our results to eliminate noisy detections, but in order to present the method in a general sense, we did not apply any further processing steps past step 5.

4.1. Quantitative analysis

In order to quantify the performance of our approach, we compare it with three existing methods: Adaptive Gaussian Thresholding method (AGT), Adaptive Mean Thresholding method (AMT) [25], and Otsu’s method [26] evaluated on the hue image. For the AGT and AMT methods, the block size was set to 11 and C was set to 2. Since these comparison methods do not take into account the region outside the background material, which would heavily influence the number of false positives, we also apply our masking operation, Step 5 from Algorithm 1 to the resulting images. It is important to emphasize that while Step 5 substantially simplifies the thresholding task for the alternative approaches, it is the greatest contributor to incorrectly segmented pixels in our proposed approach. Finally, it should be noted that no knowledge of the target bounding box is used in the evaluation.

Ground truth data was generated by hand-labeling tree versus non-tree pixels in 12 images with an image editor. The images of the quantitative results are from Datasets 3 and 5, which reflect two different imaging environments. In Dataset 3, the trees are leafless and small and the background material is taller than the trees while also covering a portion of the ground. In addition, there is a significant range of gray-level variation between the images (displayed in Figure 3). Dataset 5 shows a much bigger background unit, and the trees have leaves as well as flowers. There is no portion of the background that is on the ground (see Figure 4 for examples). Since the method was intended to segment regions that are between the camera and the blue background material, regions outside of the background unit are marked as non-tree, even if a tree is present. The exception is the top of the background, as the sky is often marked as part of the background, and recovery of the entire height of the tree is desirable.

Table 1 summarizes the performance of the comparison approaches as well as our approach in terms of the precision, recall, and the F_1 score. As the table shows, performance of the adaptive thresholding methods was not satisfactory. The performance of Otsu’s method in conjunction with our Step 5 mask, is generally higher in terms of precision but lower in terms of recall. The recall values for Otsu’s methods are lower than that of our method for 11 out of the 12 images. Although its precision is higher for 11 out of the 12 images, for Images 7-12, which correspond to Dataset 5, the precision is on average only 0.048 higher than that of our proposed approach. Nonetheless, the F_1 score is higher on average using our method, particularly

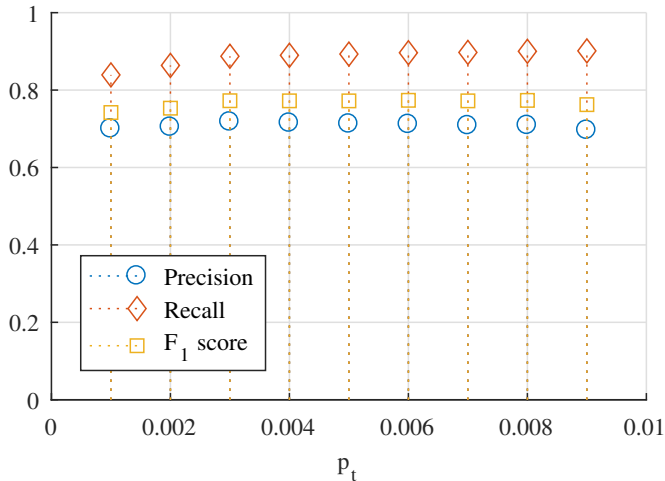


Figure 2: [Best viewed in color] Sensitivity analysis of the proposed methods to different values of p_t . Values for precision, recall, and F_1 score are displayed for the set of images used for the quantitative experiments.

for Dataset 5, which included leaves and flowers. In addition, if the mask from Step 5 is not used in the Otsu method, its mean precision is reduced to 0.413, with a corresponding F_1 scores 0.421, since its recall remains essentially unchanged at 0.720.

In order to demonstrate that the performance of the method is relatively stable with respect to the threshold p_t , Figure 2 shows a plot of the mean precision, recall, and F_1 score for a range of p_t values. As the figure indicates, the F_1 score of the method varies at most 0.016 for this range of p_t .

4.2. Qualitative analysis

The proposed method was also evaluated on images acquired from a range of conditions, including four different background unit designs in three different locations, from 2015-2017. The datasets are described in Table 2 and images and results are displayed in Figures 5-8. Examples of Dataset 3 are shown in Figures 3, while Dataset 5 examples are shown in Figure 4.

The images in these datasets, have differences in the distributions of hue components. Figure 9 shows hue histograms from the six datasets, and demonstrates that while all have peaks corresponding to the background unit, some datasets have multiple peaks, such as Dataset 2 and 4. Overall, as shown by the figures, the proposed method segments the objects of interest in the various different scenarios accurately.

4.3. Suitability in real-time automation contexts

All of the results shown in this paper were generated on a workstation with one 12-core processor and 192 GB of RAM. To the extent possible, implementation is parallelized with OpenMP. Run times for the entire dataset and on the per-image basis are shown in Table 3. These times include loading each image and writing two result images for each image in the dataset, the binary result and the original image multiplied by the binary image for visualization purposes, such as the third

and fourth columns in Figures 3-4. From Table 3, datasets containing larger images, such as Dataset 5, take approximately twice as long to run than smaller images. This relationship is not surprising considering that the area of the images in Dataset 5 is approximately $1.8\times$ the area of the images in the other datasets. In all the scenarios under consideration the low run times enable this method to be used in a real-time automation context.

5. Conclusion

This paper proposed a method to perform automatic segmentation of objects of interest in dynamic outdoor conditions. We are interested in automation scenarios in which an object of interest must be segmented from a low-texture background such as in tree reconstruction. Our method estimates a Gaussian mixture model of the low-texture background, which may include the sky, by fusing information from its color distribution and from superpixels extracted from the background. As a result, the proposed method is particularly robust to substantial variations in illumination conditions. We illustrated the performance of the proposed segmentation method in quantitative and qualitative experiments, and showed how its low run times enabled its use in real-time automation contexts.

References

References

- [1] A. Tabb, Shape from silhouette probability maps: reconstruction of thin objects in the presence of silhouette extraction and calibration error, in: Computer Vision and Pattern Recognition (CVPR), 2013 IEEE Conference on, 2013.
- [2] A. Tabb, Shape from inconsistent silhouette: Reconstruction of objects in the presence of segmentation and camera calibration error, Ph.D. thesis, Purdue University (2014).
- [3] A. Tabb, H. Medeiros, A robotic vision system to measure tree traits, in: IEEE RSJ International Conference on Intelligent Robots and Systems, 2017.
- [4] T. Bouwmans, Traditional and recent approaches in background modeling for foreground detection: An overview, Computer Science Review 1112 (2014) 31 – 66. doi:<http://dx.doi.org/10.1016/j.cosrev.2014.04.001>. URL <http://www.sciencedirect.com/science/article/pii/S1574013714000033>
- [5] C. Stauffer, W. E. L. Grimson, Adaptive background mixture models for real-time tracking, in: Computer Vision and Pattern Recognition, 1999. IEEE Computer Society Conference on., Vol. 2, IEEE, 1999.
- [6] J. Park, A. Tabb, A. C. Kak, Hierarchical data structure for real-time background subtraction, in: 2006 International Conference on Image Processing, 2006, pp. 1849–1852. doi:10.1109/ICIP.2006.312840.
- [7] A. B. Chan, V. Mahadevan, N. Vasconcelos, Generalized stauffer-grimson background subtraction for dynamic scenes, Machine Vision and Applications 22 (5) (2011) 751–766. doi:10.1007/s00138-010-0262-3. URL <http://dx.doi.org/10.1007/s00138-010-0262-3>
- [8] E. Hamuda, M. Glavin, E. Jones, A survey of image processing techniques for plant extraction and segmentation in the field, Computers and Electronics in Agriculture 125 (2016) 184 – 199. doi:<http://dx.doi.org/10.1016/j.compag.2016.04.024>. URL <http://www.sciencedirect.com/science/article/pii/S0168169916301557>
- [9] J. Byrne, S. Singh, Precise image segmentation for forest inventory, Carnegie Mellon University, The Robotics Institute, 1998.

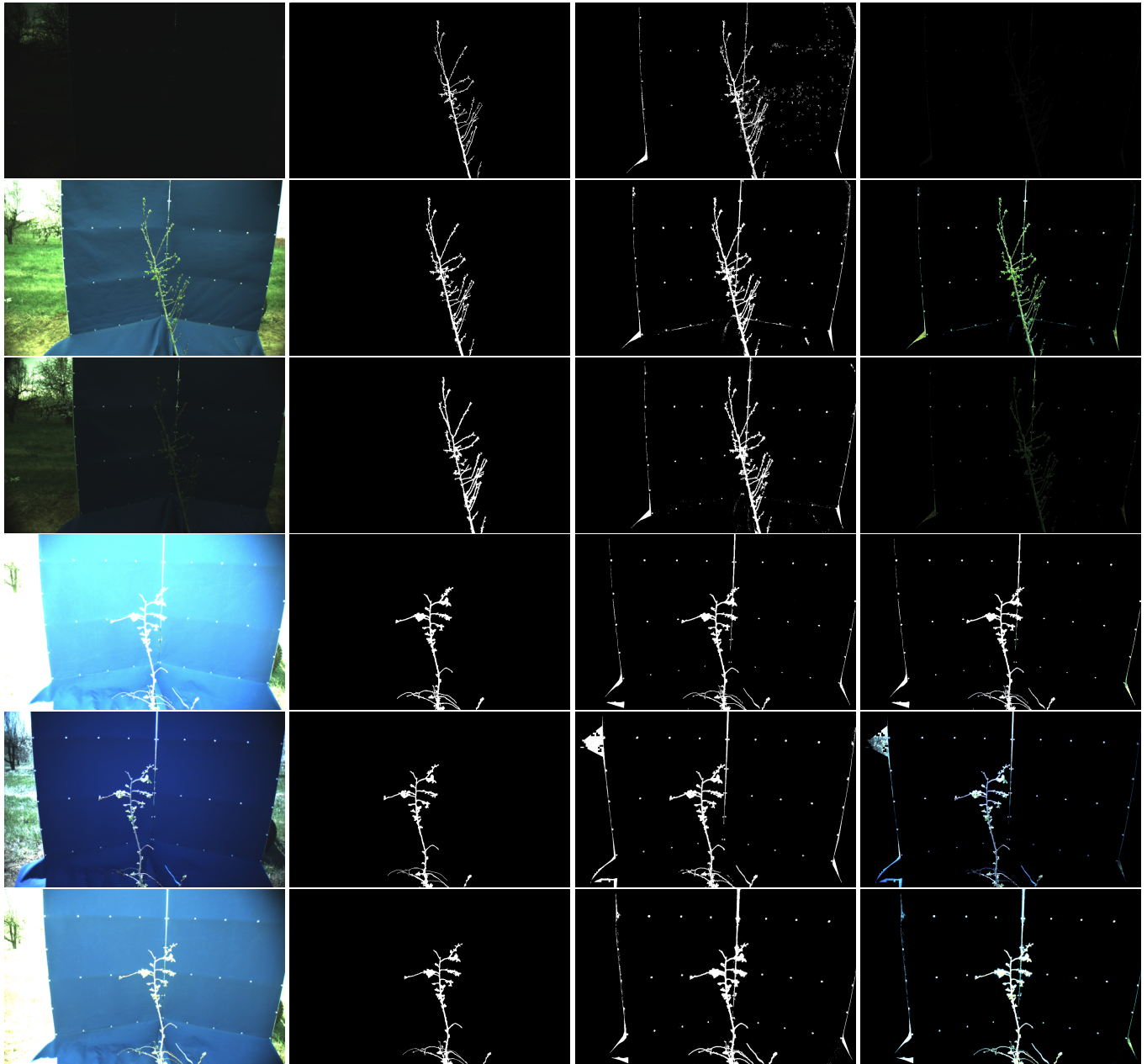


Figure 3: **[Best viewed in color]** Images of trees in front of a low-texture blue background with varying illumination levels (first column), hand-labeled ground truth (second column), the corresponding segmentations obtained using the proposed approach (third column), and the segmentation result used to mask the original image (fourth column), for the first half of the quantitative dataset (images 1-6).

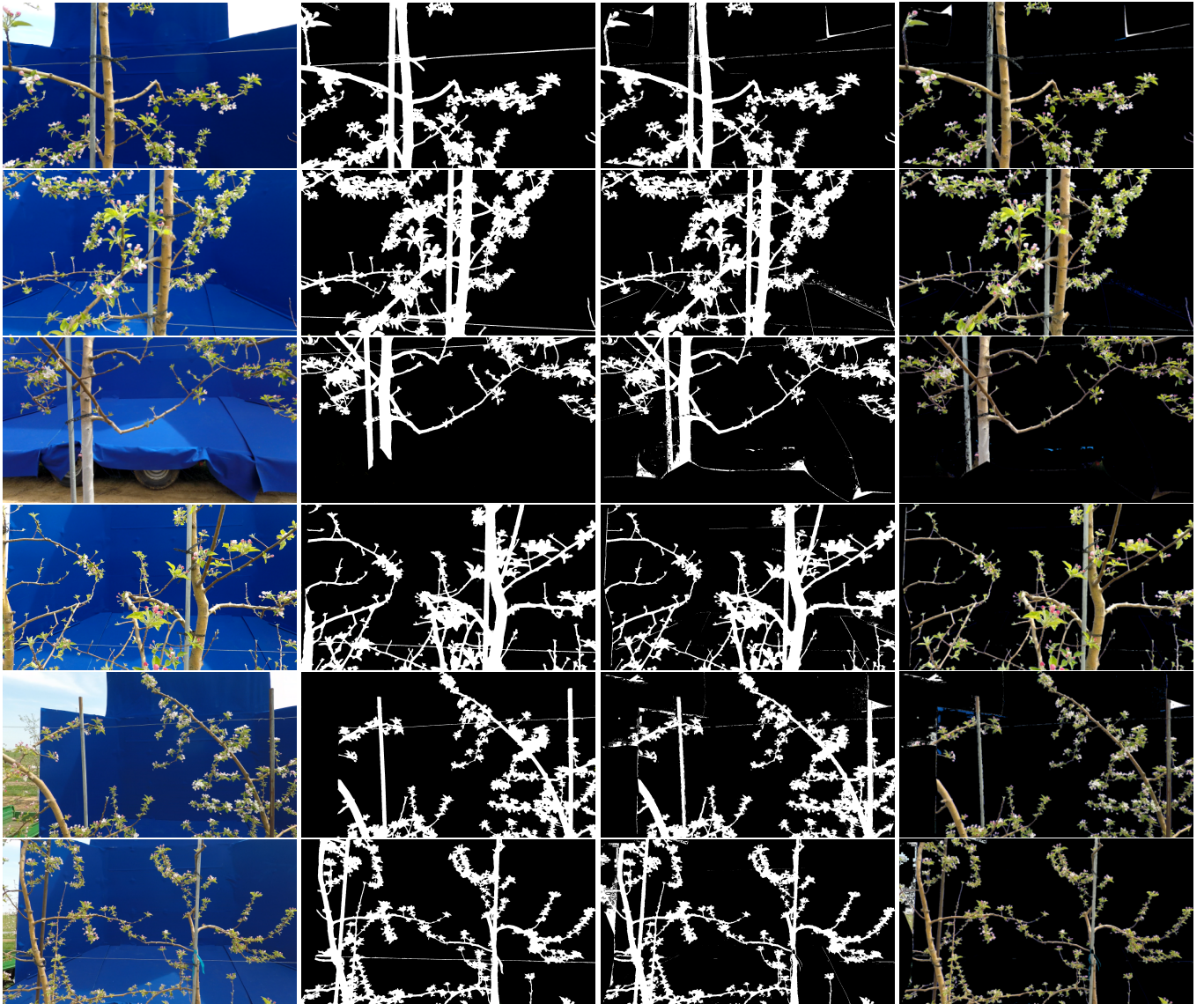


Figure 4: **[Best viewed in color]** Images of trees in front of a low-texture blue background with varying illumination levels (first column), hand-labeled ground truth (second column), the corresponding segmentations obtained using the proposed approach (third column), and the segmentation result used to mask the original image (fourth column), for the second half of the quantitative dataset (images 7-12).



Figure 5: **[Best viewed in color]** Results from Dataset 1, acquired indoors. Original images (first column), the corresponding segmentations obtained using the proposed approach (second column), and original image masked with the segmentation result (third column).

Table 1: Quantitative results comparing Adaptive Gaussian Threshold (AGT), Adaptive Mean Threshold (AMT), Otsu’s method on the hue image, and our proposed approach in precision, recall, and the F-score. Best results are shown in boldface.

Image	Precision				Recall				F-score			
	AGT	AMT	Otsu	Ours	AGT	AMT	Otsu	Ours	AGT	AMT	Otsu	Ours
1	0.022	0.025	0.204	0.361	0.505	0.591	0.799	0.739	0.042	0.048	0.325	0.485
2	0.586	0.513	0.760	0.543	0.614	0.705	0.776	0.959	0.600	0.594	0.768	0.693
3	0.085	0.086	0.687	0.593	0.519	0.596	0.678	0.846	0.146	0.151	0.683	0.697
4	0.615	0.582	0.683	0.665	0.623	0.753	0.886	0.932	0.619	0.656	0.771	0.776
5	0.468	0.461	0.693	0.385	0.419	0.451	0.362	0.903	0.442	0.456	0.476	0.540
6	0.674	0.661	0.728	0.481	0.671	0.739	0.803	0.985	0.673	0.698	0.764	0.646
7	0.894	0.856	0.977	0.960	0.258	0.333	0.684	0.861	0.400	0.480	0.805	0.907
8	0.931	0.889	1.000	0.969	0.262	0.342	0.750	0.902	0.409	0.495	0.857	0.934
9	0.805	0.761	0.934	0.876	0.320	0.405	0.681	0.896	0.458	0.529	0.787	0.886
10	0.913	0.860	0.996	0.971	0.261	0.339	0.695	0.842	0.406	0.487	0.819	0.902
11	0.818	0.775	0.981	0.884	0.305	0.398	0.745	0.906	0.445	0.526	0.847	0.895
12	0.838	0.793	0.963	0.904	0.303	0.392	0.706	0.877	0.445	0.524	0.815	0.890
Mean	0.638	0.605	0.800	0.716	0.422	0.504	0.714	0.887	0.424	0.470	0.726	0.771
Median	0.739	0.711	0.847	0.771	0.370	0.428	0.725	0.899	0.443	0.510	0.779	0.831

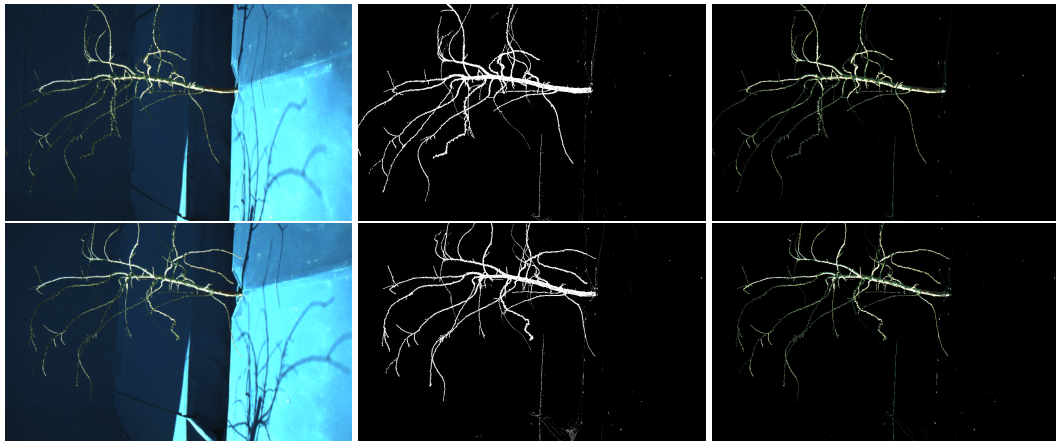


Figure 6: **[Best viewed in color]** Results from Dataset 2, acquired outdoors with significant shadow, sun, and sideways camera orientation. Original images (first column), the corresponding segmentations obtained using the proposed approach (second column), and original image masked with the segmentation result (third column).

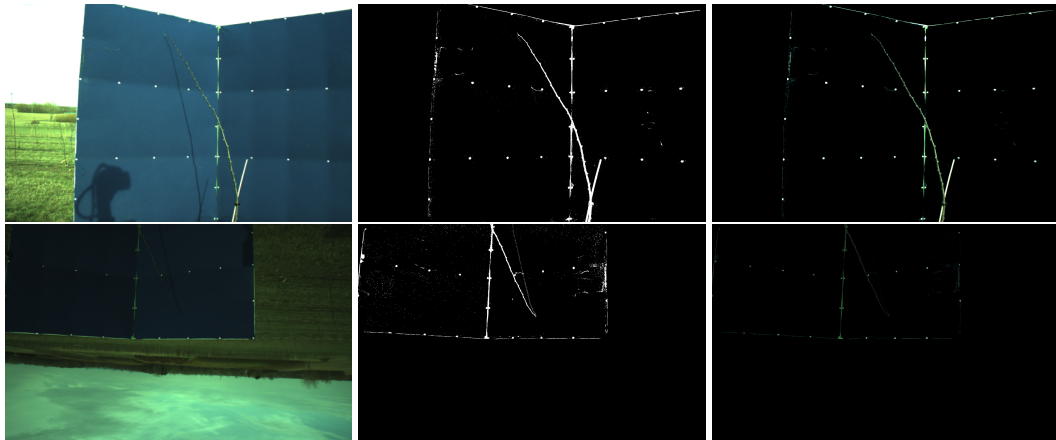


Figure 7: **[Best viewed in color]** Results from Dataset 4, acquired outdoors with significant shadows and upside down camera orientation. Original images (first column), the corresponding segmentations obtained using the proposed approach (second column), and original image masked with the segmentation result (third column).

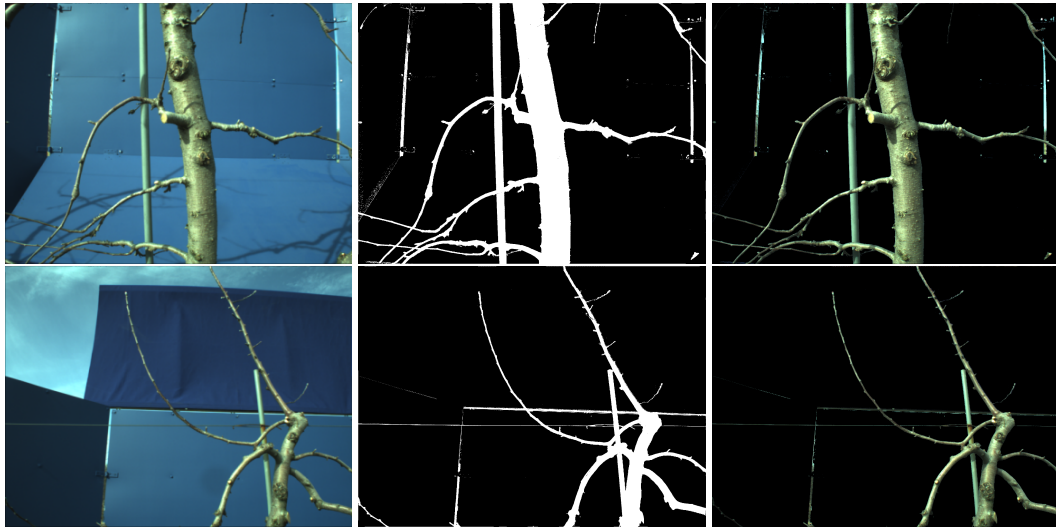


Figure 8: **[Best viewed in color]** Results from Dataset 6, acquired outdoors with a background unit with two different blue colors (fabric versus rigid painted areas). Original images (first column), the corresponding segmentations obtained using the proposed approach (second column), and original image masked with the segmentation result (third column).

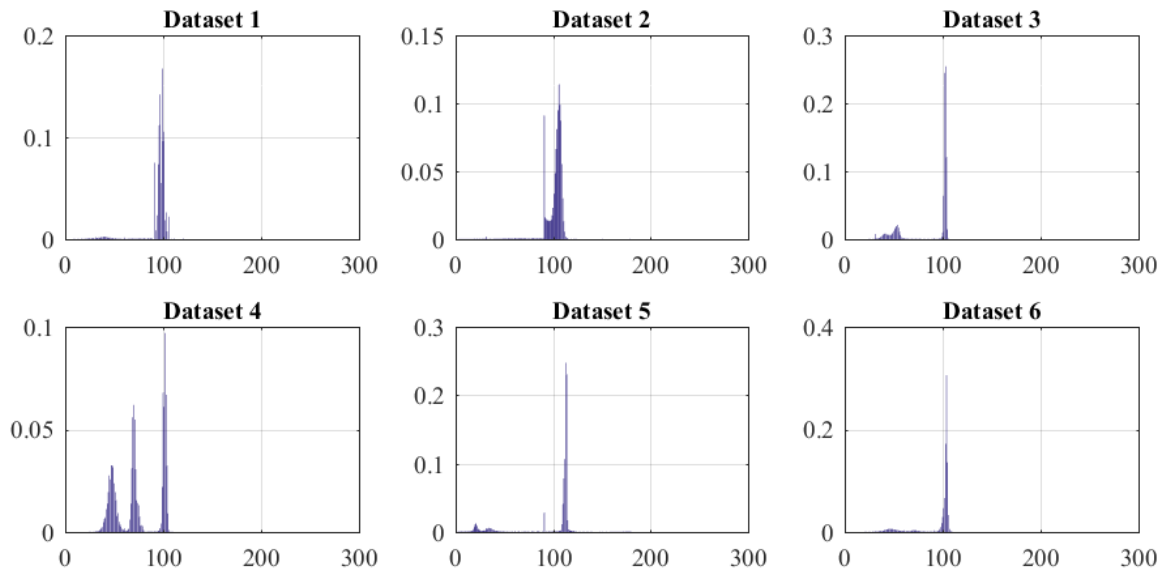


Figure 9: Examples of hue histograms from images from each of the six datasets. Although all of the histograms show a clear peak corresponding to the background unit, some datasets have multiple peaks (such as Datasets 2 and 4).

Table 2: Description of the six datasets used in this paper. The Pt. Grey camera model is BFLY-PGE-23S6C-C.

Dataset	camera model	no. cameras	environment	image size
1	Pt. Grey	2	indoor	1900 × 1200
2	Pt. Grey	2	outdoor	1900 × 1200
3	Pt. Grey	3	outdoor	1900 × 1200
4	Pt. Grey	2	outdoor	1900 × 1200
5	GoPro HERO Black	3	outdoor	2705 × 1520
6	JAI BB-500 GE	1	outdoor	1600 × 1200

Table 3: Run times of the proposed method for the six datasets, for the whole dataset as well as on an average, per-image basis.

Dataset	Number of images	Total run time (s)	average time per image (ms)
1	126	15.01	119.10
2	228	27.63	121.20
3	171	21.67	126.70
4	228	29.14	127.79
5	154	36.42	236.52
6	94	12.29	130.74

- [10] W. Ali, Tree detection using color, and texture cues for autonomous navigation in forest environment, Master’s thesis (2006).
- [11] T. Botterill, S. Paulin, R. Green, S. Williams, J. Lin, V. Saxton, S. Mills, X. Chen, S. Corbett-Davies, A robot system for pruning grape vines, *Journal of Field Robotics* (2016) n/a–n/doi:10.1002/rob.21680. URL <http://dx.doi.org/10.1002/rob.21680>
- [12] Y. Zheng, S. Gu, H. Edelsbrunner, C. Tomasi, P. Benfey, Detailed reconstruction of 3d plant root shape, in: *ICCV*, 2011.
- [13] A. Gongal, A. Silwal, S. Amatya, M. Karkee, Q. Zhang, K. Lewis, Apple crop-load estimation with over-the-row machine vision system, *Computers and Electronics in Agriculture* 120 (2016) 26–35.
- [14] J. R. Davidson, A. Silwal, C. J. Hohimer, M. Karkee, C. Mo, Q. Zhang, Proof-of-concept of a robotic apple harvester, in: *Intelligent Robots and Systems (IROS)*, 2016 IEEE/RSJ International Conference on, IEEE, 2016, pp. 634–639.
- [15] A. Silwal, A. Gongal, M. Karkee, Apple identification in field environment with over the row machine vision system, *Agricultural Engineering International: CIGR Journal* 16 (4) (2014) 66–75.
- [16] S. Amatya, M. Karkee, A. Gongal, Q. Zhang, M. D. Whiting, Detection of cherry tree branches with full foliage in planar architecture for automated sweet-cherry harvesting, *Biosystems Engineering* 146 (2016) 3–15.
- [17] W. Liu, G. Kantor, F. De la Torre, N. Zheng, Image-based tree pruning, in: *Robotics and Biomimetics (ROBIO)*, 2012 IEEE International Conference on, IEEE, 2012, pp. 2072–2077.
- [18] Q. Wang, S. Nuske, M. Bergerman, S. Singh, Automated crop yield estimation for apple orchards, in: *International Symposium on Experimental Robotics*, Quebec City, Canada, 2012.
- [19] R. Linker, A procedure for estimating the number of green mature apples in night-time orchard images using light distribution and its application to yield estimation, *Precision Agriculture* 18 (1) (2017) 59–75.
- [20] M. Van den Bergh, X. Boix, G. Roig, L. Van Gool, Seeds: Superpixels extracted via energy-driven sampling, *International Journal of Computer Vision* 111 (3) (2015) 298–314. doi:10.1007/s11263-014-0744-2. URL <http://dx.doi.org/10.1007/s11263-014-0744-2>
- [21] Opencv, <http://opencv.org/>, version 3.0.
- [22] N. Otsu, A threshold selection method from gray-level histograms, *IEEE Transactions on Systems, Man, and Cybernetics* 9 (1) (1979) 62–66. doi:10.1109/TSMC.1979.4310076.
- [23] D.-Y. Huang, C.-H. Wang, Optimal multi-level thresholding using a two-stage otsu optimization approach, *Pattern Recognition Letters* 30 (3) (2009) 275 – 284. doi:<http://dx.doi.org/10.1016/j.patrec.2008.10.003>. URL <http://www.sciencedirect.com/science/article/pii/S0167865508002985>
- [24] D. Arthur, S. Vassilvitskii, k-means++: The advantages of careful seeding, in: *Proceedings of the eighteenth annual ACM-SIAM symposium on Discrete algorithms*, Society for Industrial and Applied Mathematics, 2007, pp. 1027–1035.
- [25] R. Gonzales, R. Woods, *Digital Image Processing*, Addison-Wesley Publishing Company.
- [26] N. Otsu, A threshold selection method from gray-level histograms, *IEEE Transactions on Systems, Man, and Cybernetics* 9 (1) (1979) 62–66. doi:10.1109/TSMC.1979.4310076.